



PCCP

**Dissociation of dinitrogen on iron clusters: A detailed study  
of the Fe<sub>16</sub> + N<sub>2</sub> case.**

Journal:	<i>Physical Chemistry Chemical Physics</i>
Manuscript ID	CP-ART-10-2020-005427.R1
Article Type:	Paper
Date Submitted by the Author:	08-Dec-2020
Complete List of Authors:	Chen, Bole; Sichuan University, Institute of Atomic and Molecular Physics Gutsev, Gennady; Florida Agricultural and Mechanical University, Physics Sun, Weiguo; Sichuan University, Institute of Atomic and Molecular Physics Kuang, Xiao-Yu; Sichuan University, Institute of Atomic and Molecular Physics Lu, Cheng; University of Nevada Las Vegas, Department of Physics and Astronomy Gutsev, Lavrenty; Louisiana Tech University, Institute for Micromanufacturing Ramachandran, Bala; Louisiana Tech University, College of Engineering & Science Aldoshin, Sergey; FSBIS Institute of Problems of Chemical Physics of the Russian Academy of Sciences,

SCHOLARONE™  
Manuscripts

# Dissociation of dinitrogen on iron clusters: A detailed study of the $\text{Fe}_{16} + \text{N}_2$ case.

Bole Chen<sup>a</sup>, Gennady L. Gutsev<sup>\*b</sup>, Weiguo Sun<sup>a</sup>, Xiaoyu Kuang<sup>\*a</sup>, Cheng Lu<sup>\*c</sup>, Lavrenty G. Gutsev<sup>d,e</sup>, Sergey M. Aldoshin<sup>d</sup>, Bala R. Ramachandran<sup>e</sup>

<sup>a</sup>*Institute of Atomic and Molecular Physics, Sichuan University, Chengdu 610065, China*

<sup>b</sup>*Department of Physics, Florida A&M University, Tallahassee, Florida 32307, United States*

<sup>c</sup>*School of Mathematics and Physics, China University of Geosciences (Wuhan), Wuhan 430074, China*

<sup>d</sup>*Institute of Problems of Chemical Physics of Russian Academy of Sciences, Chernogolovka, Russia*

<sup>e</sup>*Institute for Micromanufacturing, Louisiana Tech University, Ruston, LA 71272, United States*

## Abstract

The coalescence of two  $\text{Fe}_8\text{N}$  as well as the structure of the  $\text{Fe}_{16}\text{N}_2$  cluster were studied using density functional theory with the generalized gradient approximation and a basis set of triple-zeta quality. It was found that the coalescence may proceed without an energy barrier and that the geometrical structures of resulting clusters depend strongly on the mutual orientations of the initial moieties. Dissociation of  $\text{N}_2$  is energetically favorable on  $\text{Fe}_{16}$  and nitrogen atoms share the same Fe atom in the lowest energy state of the  $\text{Fe}_{16}\text{N}_2$  species. The attachment of two nitrogen atoms leads to a decrease in the total spin magnetic moment of the ground-state  $\text{Fe}_{16}$  host by  $6 \mu_B$  due to the peculiarities of chemical bonding in the magnetic clusters. In order to gain insight in the dependence of properties on charge and to estimate bonding energies of both N atoms, we performed optimizations of  $\text{Fe}_{16}\text{N}$  and the singly charged ions of both  $\text{Fe}_{16}\text{N}_2$  and  $\text{Fe}_{16}\text{N}$ . It was found that the electronic properties of the  $\text{Fe}_{16}\text{N}_2$  cluster, such as electron affinity and ionization energy, do not appreciably depend on the attachment of nitrogen atoms but that the average binding energy per atom changes significantly. The lowering in total energy due to the attachment of two N atoms was found to be nearly independent of charge. The IR and Raman spectra were simulated for  $\text{Fe}_{16}\text{N}_2$  and its ions, and it was found that positions of the most intense peaks in the IR spectra strongly depend on charge and therefore present fingerprints of the charged states. The chemical bonding in the ground-state  $\text{Fe}_{16}\text{N}_2^{0,\pm 1}$  species was described in terms of localized molecular orbitals.

**Keywords:** cluster coalescence, molecular dissociation, magnetic moment, iron cluster, IR fingerprints

## 1. INTRODUCTION

High saturation magnetization, permeability and low coercivity make iron an extremely important material for nanocrystalline magnetic recording devices,<sup>1,2</sup> for producing nano-granular film magnetic materials,<sup>3,4</sup> permanent rare-earth-free magnets,<sup>5,6</sup> and quantum computing.<sup>7</sup> Iron forms a large number of various compounds including bulk carbides, oxides, and nitrides, which have been used for millennia.<sup>8</sup> Bulk iron nitrides possess a number of stoichiometric and non-stoichiometric phases.<sup>9</sup> In particular, the  $\alpha''$ -Fe<sub>16</sub>N<sub>2</sub> phase has received significant attention since it was reported<sup>10</sup> to show a large saturation magnetization of 2.8-3.0 T. Subsequently, Sugita et al.<sup>11</sup> have synthesized  $\alpha''$ -Fe<sub>16</sub>N<sub>2</sub> single-crystal films on the substrates of In<sub>0.2</sub>Ga<sub>0.8</sub>As (001) by the molecular beam epitaxy method and found a saturation magnetization value of 2.9 T, which further confirmed that this iron nitride phase possesses a large saturation magnetization. Iron-catalysis plays a special role in agriculture where large-scale production of ammonia uses the Haber-Bosch process. This economically important reaction is based on the use of iron nanoparticles as the catalysts; however, the mechanism of the H<sub>2</sub> and N<sub>2</sub> conversion into NH<sub>3</sub> is to this day not fully understood.

These experimental findings elevated interest in studying the magnetic properties of iron nitrides. Tanaka et al.<sup>12</sup> calculated the band structures and magnetic properties of two proposed phases of Fe<sub>16</sub>N<sub>2</sub>. In their work, the magnetic moments obtained in calculations of both phases were in serious disagreement with the experimental data. The discrepancy has been attributed to both the limitations of the theoretical simulations and the uncertainty in the Fe-N materials used in experiments. Another theoretical study of the giant saturation magnetization of Fe<sub>16</sub>N<sub>2</sub> was based on the LSDA+*U* method. There it was found that a fairly large Hubbard *U* value is required to achieve a high magnetization value. The authors concluded<sup>13</sup> that the giant saturation magnetization could be related to the coexistence of the localized and itinerant electron states. Sims et al.<sup>14</sup> obtained for Fe<sub>16</sub>N<sub>2</sub> the average local spin magnetic moments of 2.9  $\mu_B$  using a hybrid density functional theory (DFT) method, 2.6–2.7  $\mu_B$  within the GW approximation, and 2.7  $\mu_B$

using a DFT method with the generalized gradient approximation (GGA) for the exchange-correlation functional and a Hubbard  $U$  parameter (DFT-GGA-U).

The continuous miniaturization of magnetic-based devices along with requirements for the materials with high magnetic moments led to an increased interest in the iron-based nanoparticles. In the past two decades, great progress has been achieved in the experimental and theoretical study of small and medium-sized iron clusters,<sup>15,16,17,18,19,20,21,22,23,24,25,26,27,28,29</sup> in which the magnetic properties of the clusters were found to be highly size-dependent. The peaks at  $n = 7, 13, 15, 19,$  and  $23$  in the mass spectra of  $\text{Fe}_n$  obtained by Sakurai *et al.*<sup>30</sup> possessed higher intensities than their nearest neighbors, and these  $n$  numbers were referred to as “magic numbers”. The results of theoretical studies on iron clusters generally agree with this experimental finding.

Interactions of neutral and charged iron clusters with different small chemical species have also been extensively studied.<sup>31</sup> Recent publications include the studies on the iron-pyrene cluster anions,<sup>32</sup> the absorption of CO on  $\text{Fe}_n^+$  ( $n = 4-17$ ),<sup>33</sup> absorption and dissociation of ammonia on small iron clusters,<sup>34</sup> and the absorption and reduction of CO on neutral and charged iron clusters.<sup>35</sup> It was found that dissociation of water molecules on iron clusters depends<sup>36</sup> on the cluster size as well as on the doping of iron clusters with other  $3d$ -metal atoms.<sup>37</sup> Interactions of hydrocarbons with iron clusters are represented by studies of complexes of iron cluster cations with methane<sup>38</sup> and ethylene<sup>39</sup> as well as of benzene<sup>40</sup> adsorption on small iron clusters. The recent investigations of the interactions of iron clusters with the smallest chemical species, atoms, are presented by an experimental work<sup>41</sup> on  $\text{Fe}_4\text{O}^-$  and  $\text{Fe}_5\text{O}^-$  and a theoretical study<sup>42</sup> on  $\text{Fe}_n\text{C}^{0,\pm 1}$  ( $n \leq 13$ ).

Interactions of nitrogen atoms and dimers with iron clusters have received less attention, probably because the  $\text{N}_2$  dimer possesses a very large bond energy of 9.76 eV. According to the results of mass-spectrometry studies,<sup>43</sup> the activation of the  $\text{N}_2$  bond occurs at higher collision energies and the formation of both mononitride  $\text{Fe}_n\text{N}^+$  and dinitride  $\text{Fe}_n\text{N}_2^+$  cluster ions have been observed. The smallest observed

$\text{Fe}_n\text{N}_2^+$  was for  $n = 4$  and the production of  $\text{Fe}_n\text{N}_2^+$  became prominent for  $n \geq 16$ . Spectroscopic constants of the smallest mononitride cluster,  $\text{FeN}$ , were obtained by several experimental groups.<sup>44,45,46</sup>

The computational studies on  $\text{Fe}_n\text{N}$  and  $\text{Fe}_n\text{N}_2$  are quite scarce, with the sole exception of the  $\text{FeN}$  dimer which was the subject of a number of publications.<sup>47</sup> It was found<sup>48</sup> that dissociation of  $\text{N}_2$  is energetically favorable for the neutral and charged  $\text{Fe}_4\text{N}_2$  clusters, whereas  $\text{N}_2$  attaches to a slightly smaller  $\text{Fe}_3$  cluster in an end-on position.<sup>49</sup> The structure and electronic properties of neutral and singly charged  $\text{Fe}_n\text{N}$  were recently studied<sup>50</sup> in the range of  $1 \leq n \leq 7$ , and it was found that  $\text{Fe}_4\text{N}$  and  $\text{Fe}_6\text{N}$  are the most stable in the series. In our recent work<sup>51</sup> on modifications of properties of the  $\text{Fe}_8$  and  $\text{Fe}_8^-$  clusters via interactions with a single N atom, it was shown that the nitrogen absorption leads to distortions of the initial cluster geometries but does not seriously affect the total spin magnetic moment.

In the present work, we extend our previous study on  $\text{Fe}_8\text{N}$  to its dimer counterpart  $\text{Fe}_{16}\text{N}_2$  to gain insight on the behavior of  $\text{N}_2$  after its dissociation on the  $\text{Fe}_{16}$  cluster. We performed a systematic study on the structure, geometry and bonding patterns in the neutral, anionic and cationic  $\text{Fe}_{16}\text{N}_2$  clusters. Our search for the ground state of the neutral  $\text{Fe}_{16}\text{N}_2$  was performed in the whole range of possible spin multiplicities  $1 \leq 2S + 1 \leq 55$  using a large number of various trial geometrical structures. For comparison and evaluation of binding energies of the N atoms, the neutral, anionic and cationic  $\text{Fe}_{16}\text{N}$  clusters were also optimized. The chemical bonding patterns were explored using Adaptive Natural Density Partitioning (AdNDP) method<sup>52</sup> which allows for the construction of multicenter bonding molecular orbitals.

## 2. COMPUTATIONAL DETAILS

Our calculations were carried out using all-electron spin-polarized density functional theory with the generalized gradient approximation as implemented in the GAUSSIAN 09 program.<sup>53</sup> We have used the BPW91 functional composed of the Becke exchange<sup>54</sup> and Perdew-Wang correlation<sup>55</sup> combined with the 6-311 + G\* basis set of triple- $\zeta$  quality.<sup>56</sup> Smaller basis sets are considered unreliable in the computations of transition metal compounds.<sup>57</sup> Despite the age of the BPW91 method and the development of many exchange-correlation functionals in the intervening years, it remains to be one of

the most reliable methods when dealing with compounds containing multiple transition metal atoms. For the clusters containing iron atoms, it was found that there is a close agreement between the results of BPW91 computations and the experimental data obtained by different methods, mainly via mass and photoelectron spectroscopies. The illustrative examples include the  $\text{Fe}_n\text{O}$  and  $\text{Fe}_n\text{O}^-$  series<sup>58</sup> and the  $\text{Fe}_n^{+,0,-}$  series.<sup>59</sup> The performance assessment of different pure and hybrid DFT approaches was made using the results of computations of the large number of different transition metal oxides, and the BPW91 method was found to be one of the most suitable methods.<sup>60,61,62,63,64</sup> Capabilities of reproducing antiferromagnetic states in the  $\text{Fe}_8-\text{Fe}_8\text{O}_8$  pair were tested<sup>65</sup> for several DFT methods: BPW91, PW91,<sup>66</sup> PBE,<sup>67</sup> revTPSS,<sup>68</sup> and M06L.<sup>69</sup> Whereas the results of computations obtained for the bare iron clusters were practically independent of the method used, the performance of both revTPSS and M06L was unsatisfactory for the antiferromagnetic states of the iron oxide cluster. Among all three other congener methods, the BPW91 method was found to be more reliable.

The trial geometries were generated in several ways. The first set was obtained using the CALYPSO global search approach<sup>70</sup>, the second set was prepared by placing two nitrogen atoms onto two symmetrically nonequivalent faces on the surface of the ground-state  $\text{Fe}_{16}$  cluster since such positions seems to be preferred.<sup>71</sup> We also tested a  $\text{N}_2$  dimer situated on the cluster surface in the side-on and end-on positions. The geometries obtained by insertion of two separated N atoms as well as an  $\text{N}_2$  dimer were also among the trial structures. Optimizations of the states with each trial geometry were started with the maximal spin multiplicity of  $2S + 1 = 55$  which is slightly larger than the spin multiplicity of the  $\text{Fe}_{16}$  cluster and then we moved down in spin multiplicity using the final wavefunction of the previous spin multiplicity state as an initial guess for the current one.

Each geometry optimization was followed by computations of the harmonic vibrational frequencies to confirm that the optimized geometry corresponds to a stationary state. The convergence threshold for total energy and the force threshold were set to  $10^{-8}$  eV and  $10^{-3}$  eV/Å, respectively. Local total spin magnetic moments on atoms were obtained using the natural atomic orbital populations (NAO)

from the NBO analysis.<sup>72</sup>

### 3. RESULTS OF COMPUTATIONS

We start by considering the coalescence of two  $\text{Fe}_8\text{N}$  clusters depending on the mutual orientations of the moieties. Next, we proceed with searching for the lowest energy isomers of the neutral and singly charged  $\text{Fe}_{16}\text{N}_2$  clusters. Special attention was paid to the ferrimagnetic states formed due to the superexchange via  $-\text{N}-\text{Fe}-\text{N}-$  bridges. For comparison purposes, we optimized the lowest energy states of the neutral and singly charged  $\text{Fe}_{16}\text{N}$  clusters and compare the electron affinities, ionization energies and binding energies of  $\text{Fe}_{16}$ ,  $\text{Fe}_{16}\text{N}$  and  $\text{Fe}_{16}\text{N}_2$ . We also calculated and compared the total energies of the lowest energy states of  $\text{Fe}_{16}$  and  $\text{Fe}_{16}\text{N}_2$  as a function of the total spin magnetic moment when moving down in the spin multiplicity from the ferromagnetic high-spin states to the antiferromagnetic singlet states. The dipole electric polarizabilities of  $\text{Fe}_{16}$  and  $\text{Fe}_{16}\text{N}_2$  were also compared and the IR and Raman spectra were simulated for neutral and singly charged  $\text{Fe}_{16}\text{N}_2$ . Finally, the bonding patterns in the  $\text{Fe}_{16}\text{N}_2$  cluster are discussed.

#### 3.1. Coalescence of two $\text{Fe}_8\text{N}$ clusters

The coalescence of two  $\text{Fe}_8\text{N}$  clusters whose ground-state geometrical structures were found in our previous work<sup>51</sup> was considered first using the standard approach of searching for transition states when the clusters are separated by the 7.0 Å. Such a separation distance is arbitrary and was chosen on the assumption that the clusters interact weakly with each other at such a distance and the mutual orientations are not hindered whereas the basis sets of both clusters overlap sufficiently enough. To gain insight into the dependence of coalescence on the mutual orientation of the moieties, we considered three initial cluster positions; namely, when both N atoms are directed toward one another (the N–N case), when the second cluster position is obtained by translating the first cluster without rotations (the N–Fe case), and when both N atoms are on the opposite sides (the Fe–Fe case). Using the same initial cluster configurations, we have also performed direct optimizations in order to check if coalescence may proceed

without an energetic barrier. The results of direct optimizations are presented in Figure 1 whereas the results for coalescence proceeding via transition states are displayed in Figure S1.

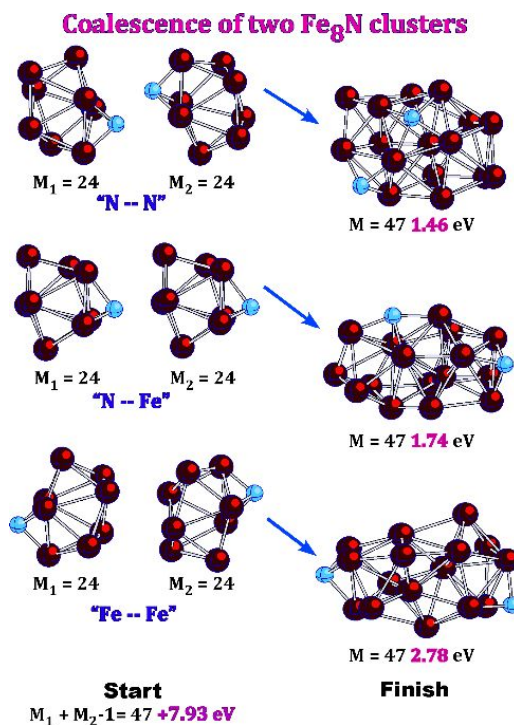


**Figure 1.** Coalescence of two ground-state Fe<sub>8</sub>N clusters simulated by the direct optimizations. All total energies are given with respect to the total energy of the ground-state Fe<sub>16</sub>N<sub>2</sub> cluster. The distance between Fe<sub>8</sub>N clusters of 7.0 Å is significantly reduced in order to make more compact images and M denotes the spin multiplicity 2S + 1.

As may be seen in Figures 1 and S1, the geometrical topologies of the final states obtained in both ways are different but the relative energies of the isomers belonging to the same initial cluster positions are quite similar. Note that the lowest energy isomers in both cases correspond to the N–N case where two N atoms are attached in the bridged –N–Fe–N– configurations. On the whole, one may conclude that coalescence may proceed spontaneously and that the geometries of the final states depend on the mutual orientation of the Fe<sub>8</sub>N clusters.

The geometry dependence of coalesced clusters on the initial orientation of two moieties is even more evident in the case of two Fe<sub>8</sub> clusters. As can be seen in Figure 2, the coalescence may result into the ground-state Fe<sub>16</sub> cluster at one mutual orientation of the initial clusters and may result into a quasi-

linear structure composed of  $\text{Fe}_6$  octahedra connected via their edges at another orientation. In the latter case, the corresponding state is substantially higher in total energy than the ground state.

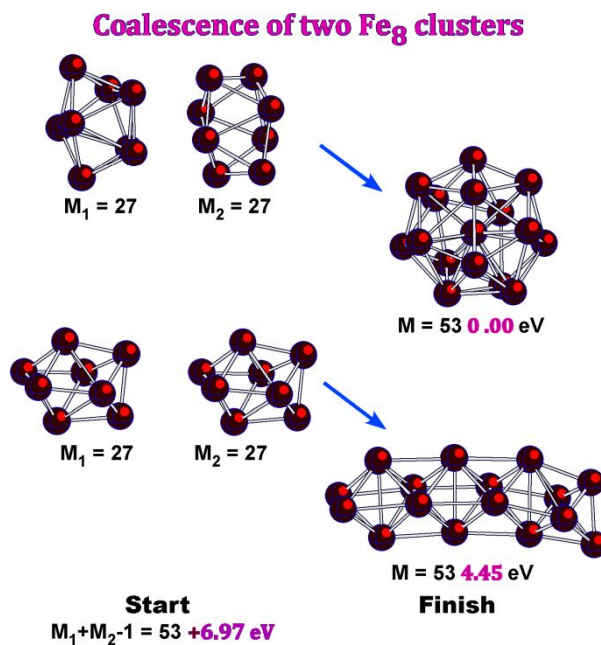


**Figure 2.** Coalescence of two ground-state  $\text{Fe}_8$  clusters simulated by the direct optimizations. All total energies are given with respect to the total energy of the ground-state  $\text{Fe}_{16}$  cluster. The distance between  $\text{Fe}_8$  clusters of 7.0 Å is significantly reduced in order to make a more compact presentation and  $M$  denotes the spin multiplicity  $2S + 1$ .

Our results on coalescence of both  $\text{Fe}_8\text{N}$  and  $\text{Fe}_8$  clusters show that the geometrical structures of the resulting dimers strongly depend on the initial mutual orientations of coalescing moieties. The dimerization energies defined as the difference between the sum of total energies of the initial ground-state  $\text{Fe}_8$  and  $\text{Fe}_8\text{N}$  clusters and total energies of the ground-state  $\text{Fe}_{16}$  and  $\text{Fe}_{16}\text{N}_2$  clusters are 6.97 eV and 7.93 eV, respectively. This means that the nitridation stabilizes the  $\text{Fe}_{16}$  cluster.

### 3.2. Optimizations of the $\text{Fe}_{16}\text{N}_2$ Isomers

Overall, we tested more than 60 selected geometrical structures as possible candidates for the ground state geometry of the  $\text{Fe}_{16}\text{N}_2$  cluster. For each trial geometry, most optimizations were started with the spin multiplicity of the ground state of the bare  $\text{Fe}_{16}$  cluster,  $2S + 1 = 53$ , and moved down in the spin multiplicity using the electronic densities from the previous step as guesses for the next step. In some cases, the optimizations were started with  $2S + 1 = 55$  to make sure that nitridation cannot result in the

lowest total energy states with the spin multiplicity exceeding that of the initial ground-state  $\text{Fe}_{16}$  cluster. It was found that total energy decreases in all cases to the  $2S+1$  value ranging from 43 to 49, with  $2S+1 = 47$  being most common, and then rises up when the multiplicity is lowered further. It was observed that the states with geometries where both N atoms are bound to the same Fe atom are generally lower in total energy than the other states. Such a preference can be related to a kind of superexchange mechanism via the  $-\text{N}-\text{Fe}-\text{N}-$  bridges which is similar to the one previously found for the  $\text{Cr}_2\text{O}_2$ ,<sup>73</sup>  $\text{Mn}_2\text{O}_2$ ,<sup>74</sup>  $\text{Fe}_2\text{O}_2$ ,<sup>75</sup> and  $\text{Co}_2\text{O}_2$ <sup>76</sup> clusters. The superexchange phenomenon arises from the specific type of bonding in late  $3d$ -metal atoms possessing a half-filled  $3d$  subshell which is chemically inert. Only  $4s$  and virtual  $4p$  atomic orbitals can participate in the bonding in the spin representation to which this half-filled subshell  $3d$  belongs. When an  $sp$  atom is inserted between two  $3d$ -metal atoms, it can form bonds in both spin representations indiscriminatory which allows the spins of one filled half-shell to change orientation with respect to another one according to the Pauli repulsion principle. The total energy change when the mutual orientations of the  $3d$  half-shells changes from ferromagnetic to antiferromagnetic is relatively small and is in the range of 0.1–0.2 eV according to the results of our computations for linear  $\text{Mn}-\text{O}-\text{Mn}$  and  $\text{Fe}-\text{O}-\text{Fe}^+$ .<sup>74</sup> Peculiarities of the bonding patterns in the ferromagnetic and antiferromagnetic states were considered in detail in the case of the  $\text{Fe}_2\text{O}_2$  cluster.<sup>77</sup> Figure 3 illustrates the superexchange effect for four lowest energy states including the ground state of  $\text{Fe}_{16}\text{N}_2$ . As can be seen, the difference between total energies of the ferromagnetic states and their ferrimagnetic counterparts are small and the ferrimagnetic state of the third in energy isomer is lower in total energy than the ferrimagnetic state. It should, of course, be expected that the superexchange interactions are much more complicated than in simple linear cases since the nitrogen atoms are bound to several iron atoms as well as the bridge Fe atoms are bounded to other neighbors.

The dissociation of  $\text{N}_2$  on the surface of both ground-state  $\text{Fe}_{16}$  cluster and its isomers (shown in Figure S2) was observed to always lead to a decrease in the spin multiplicity with respect to that of an initial  $\text{Fe}_{16}$  isomer. The non-dissociative end-on attachment of  $\text{N}_2$  decreases the spin multiplicity by two

as can be seen in Figure S3 and the corresponding state is above the ground state of  $\text{Fe}_{16}\text{N}_2$  by only 0.42 eV. The side-on attachment is less energetically favorable; the lowest energy state of an isomer with a side-on geometry has a multiplicity of  $2S + 1 = 49$  and is higher in total energy than the ground state by 0.96 eV. Total energies of isomers with end-on and side-on attachments were found to weakly depend on their position on the  $\text{Fe}_{16}$  surface.

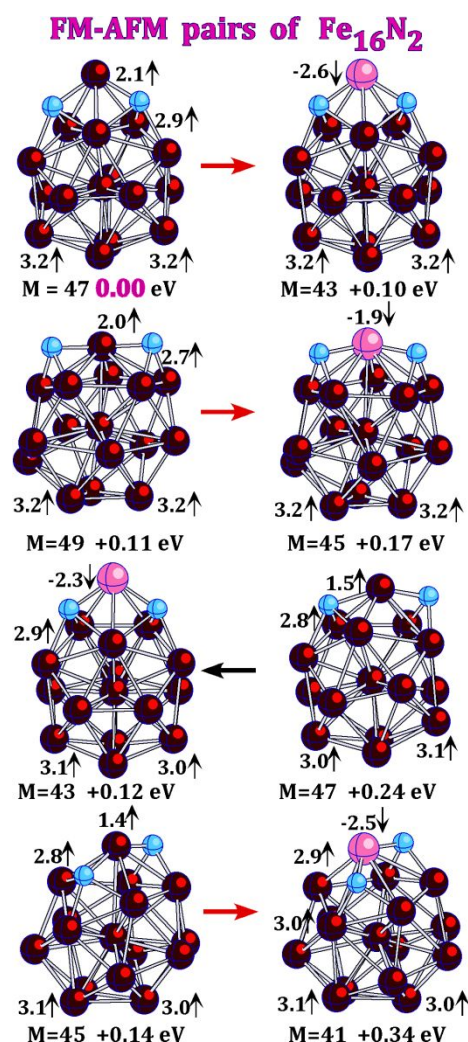


**Figure 3.** Four lowest energy isomers of  $\text{Fe}_{16}\text{N}_2$  and their ferrimagnetic counterparts. M stands for the spin multiplicity  $2S+1$ , total energies are given with respect to that of the ground state, and the local spin magnetic moments are in Bohr magneton.

The possibility of N and  $\text{N}_2$  encapsulation was probed by incorporating a single N atom, two separated N atoms, and the intact  $\text{N}_2$  dimer inside the ground-state  $\text{Fe}_{16}$  cluster. The results of optimizations of trial geometries with such distributions are shown in Figure 4. As one can observe, both

single N atom and two separated N atoms are always pushed out to the cluster surface, while the N<sub>2</sub> dimer remains inside the iron shell formed during the optimizations, although its total energy is significantly higher than total energies of states with dissociative attachment of the nitrogen dimer. The figure shows the results obtained for states with  $2S + 1 = 51$ ; similar trends were found for other spin multiplicities in the range of  $47 \leq n \leq 53$ .

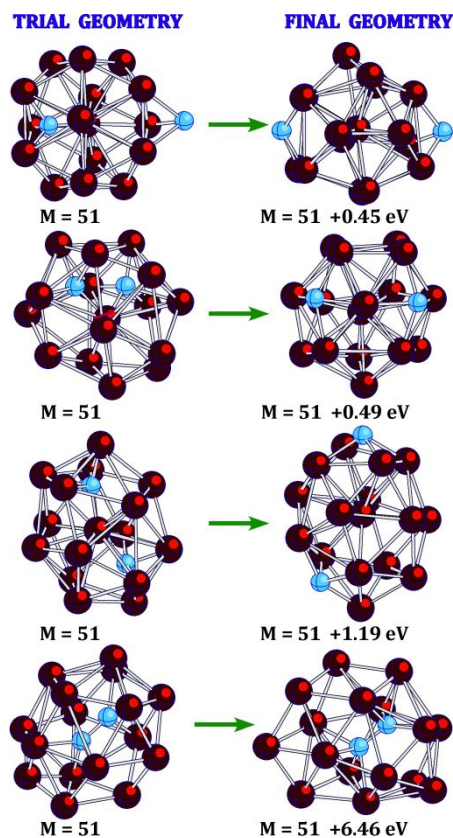


**Figure 4.** The results of optimizations of Fe<sub>16</sub>N<sub>2</sub> states with the spin multiplicity  $M=2S+1=51$  whose trial geometries contain one internal N atom and the second N on the cluster surface (the top panel), when both N atoms are inside the cluster (two middle panels), and when the dimer N<sub>2</sub> is inside the cluster (the bottom panel). The total energies are with respect to the total energy of the ground-state Fe<sub>16</sub>N<sub>2</sub> cluster.

### 3.3. The lowest energy states of Fe<sub>16</sub>N<sub>2</sub><sup>0,±1</sup> and Fe<sub>16</sub>N<sup>0,±1</sup>

In order to gain insight into the dependence of properties of the Fe<sub>16</sub>N<sub>2</sub> cluster on charge, we have optimized the anion and cation states using the geometrical structures of the first ten low-lying isomers of neutral Fe<sub>16</sub>N<sub>2</sub> in a wide range of spin multiplicities around  $2S + 1 = 48$ , which is than the ground-state multiplicity of Fe<sub>16</sub>N<sub>2</sub>. The results of our search for the lowest states are shown in Figure 5 where the

neutral states are presented for comparison. Both the attachment and detachment of an electron leads to an increase in the spin multiplicity of the neutral parent by one. The anion geometry presents a strongly distorted neutral geometrical structure whereas the cation geometry is presented by a nearly unperturbed neutral geometry. The first flip of the local spin magnetic moments occurs at the Fe atoms connected to both nitrogens in all the cases studied. This flip results into the change of the spin multiplicity by four which corresponds to a decrease in the total spin magnetic moment of a cluster by  $4 \mu_B$ . The difference in total energies of the states in the ferro-ferrimagnetic pairs decreases from 0.10 eV in the neutral case to 0.03 eV for the anion pair.

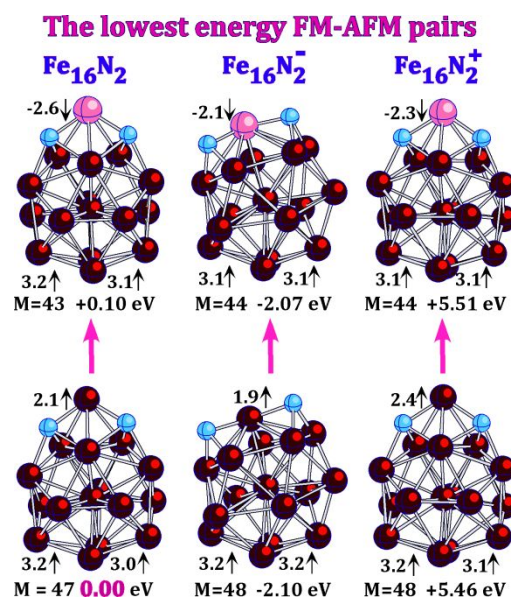


**Figure 5.** The lowest energy states of  $\text{Fe}_{16}\text{N}_2$  and its singly charged ions along with the corresponding states with the first flip of the local spin magnetic moments. M stands for the spin multiplicity  $2S+1$ , total energies are given with respect to that of the ground state of  $\text{Fe}_{16}\text{N}_2$ , and the local spin magnetic moments are in Bohr magneton.

To assess the binding energies of separated nitrogen atoms in the  $\text{Fe}_{16}\text{N}_2^{0,\pm 1}$  species, we have optimized the  $\text{Fe}_{16}\text{N}^{0,\pm 1}$  species as well. Their trial geometries were obtained by stripping one N atom from the  $\text{Fe}_{16}\text{N}_2$  geometrical structures and the range of spin multiplicities was restricted to  $42 \leq 2S + 1 \leq 54$ , since the further decrease or increase in the spin multiplicity led to the states with substantially higher total energies. The results of optimizations are presented in Figure 6. As can be seen, all iron frameworks

have topologies similar to that of the ground-state bare  $\text{Fe}_{16}$  cluster and the spin multiplicities differ by one from the spin multiplicities of the corresponding  $\text{Fe}_{16}\text{N}_2^{0,\pm 1}$  clusters. It is worth to note that the first flip energies presented in Figure 6 are substantially larger compared to those in the  $\text{Fe}_{16}\text{N}_2$  series.

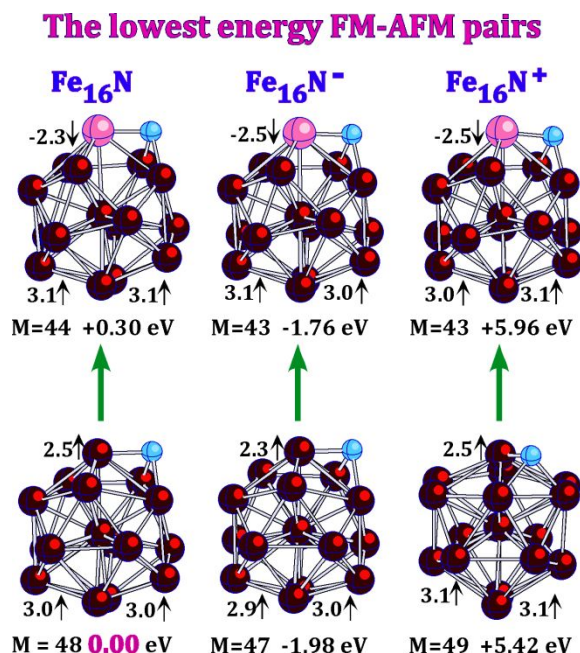


**Figure 6.** The lowest energy states of  $\text{Fe}_{16}\text{N}$  and its singly charged ions along with the corresponding states with the first flip of the local spin magnetic moments.  $M$  stands for the spin multiplicity  $2S+1$ , total energies are given with respect to that of the ground state of  $\text{Fe}_{16}\text{N}$ , and the local spin magnetic moments are in Bohr magneton.

### 3.4. Total energy as a function of the total spin magnetic moment

The total magnetic moment of a species is defined as  $\boldsymbol{\mu} = (2\mathbf{S} + \mathbf{L})$  where  $\mathbf{L}$  and  $\mathbf{S}$  are the total angular and spin moments, respectively, and is measured in Bohr magnetons,  $\mu_B$ . The total spin magnetic moment,  $M = 2S\mu_B$ , is computed as  $[n_\alpha - n_\beta]\mu_B$ , where  $n_\alpha$  and  $n_\beta$  are the numbers of the majority and minority spin electrons, respectively. The local spin magnetic moments on atoms are considered to be equal to the excess spin densities obtained using the NAO populations.

Using the geometrical structures of the ground-state  $\text{Fe}_{16}$  and  $\text{Fe}_{16}\text{N}_2$  clusters as initial ones we performed geometry optimizations for all states of both series in the range of  $1 \leq 2S + 1 \leq 61$ . The total energies obtained in these optimizations are presented in Figure 7 as a function of the total spin magnetic

moment. As can be seen, the total energy increases sharply when the spin multiplicity is larger than the ground-state value in the case of the bare iron cluster and not so fast in the case of the  $\text{Fe}_{16}\text{N}_2$  cluster. Total energies rise when the spin multiplicity decreases with the  $\text{Fe}_{16}\text{N}_2$  curve slowly approaching the  $\text{Fe}_{16}$  curve from below until they nearly merge at  $2S + 1 = 3$  and next moving slightly apart at the singlet states.

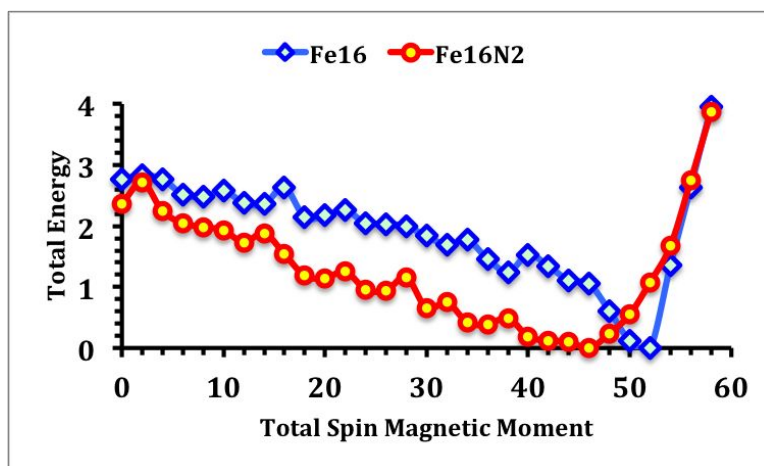


**Figure 7.** Total energies of the  $\text{Fe}_{16}$  and  $\text{Fe}_{16}\text{N}_2$  states originating from the corresponding ground states as a function of the total spin magnetic moments (in Bohr Magnetons). All total energies (in eV) are with respect to the corresponding ground-state total energies.

The singlet states of both clusters are presented in Figure 8. As can be seen, the atoms with the mutually parallel local spin moments are not randomly placed but form two groups with the spin-up and spin-down local spin magnetic moments similar to what was previously found for bare Mn clusters.<sup>78,79,80</sup> In a sense, one may consider the atoms with the parallel spin coupling as forming two nanodomains. The reason for such a segregation can be related to the peculiarities in the bonding between magnetic atoms, when  $3d-3d$  bonds can be formed between atoms whose spin magnetic moments are parallel. Between atoms with the antiparallel spin coupling, bonds can be formed only from  $4s$  and  $4p$  atomic orbitals. Therefore, the chemical bonding between atoms with the antiparallel spin coupling is generally weaker than the chemical bonding between atoms with the parallel spin coupling. The total effect of two types of chemical bonding in the antiferromagnetic singlet states, i.e., inside the two domains and between the domains, is reflected in an increase in total energy by 2.74 eV and 2.33 eV in the singlet states of the  $\text{Fe}_{16}$  and  $\text{Fe}_{16}\text{N}_2$  clusters, respectively, with respect to their lowest energy ferromagnetic states.

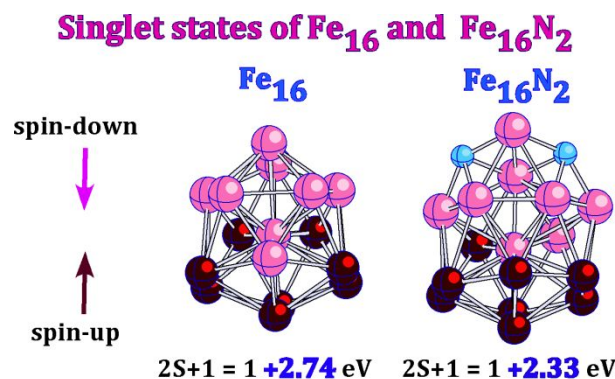


**Figure 8.** The singlet states of Fe<sub>16</sub> and Fe<sub>16</sub>N<sub>2</sub> obtained by moving down in the spin multiplicity beginning with the corresponding ground states.

### 3.5. Polarizabilities of Fe<sub>16</sub> and Fe<sub>16</sub>N<sub>2</sub>

The dipole electric polarizability is an important property of a chemical compound since it is related to the response of the compound to external electric fields. The static dipole electric polarizabilities correspond to the coefficients in the Taylor expansions of total energy perturbed by a weak uniform external static electric field<sup>81</sup>

$$E^p = E^0 - \sum_{\alpha} \mu_{\alpha} F_{\alpha} - \frac{1}{2} \sum_{\alpha, \beta} \alpha_{\alpha\beta} F_{\alpha} F_{\beta} - \frac{1}{6} \sum_{\alpha, \beta, \gamma} \beta_{\alpha\beta\gamma} F_{\alpha} F_{\beta} F_{\gamma} + \dots \quad (1)$$

where  $E^p$  is the perturbed total energy,  $F$  is a static electric field,  $E^0$  is the total energy in the absence of the field,  $\mu_{\alpha}$  are the components of the permanent dipole moment,  $\alpha_{\alpha\beta}$  are the components of the static dipole electric polarizability tensor and  $\beta_{\alpha\beta\gamma}$  represent the second order nonlinear polarizabilities. Greek subscripts denote the  $x$ ,  $y$ , and  $z$  space variables. The mean electric polarizability  $\bar{\alpha}$  is the trace of the static dipole electric polarizability tensor:

$$\bar{\alpha} = \frac{1}{3} (\alpha_{xx} + \alpha_{yy} + \alpha_{zz}) \quad (2)$$

The electric polarizabilities were computed for the states with the same topologies as those of the ground states of Fe<sub>16</sub> and Fe<sub>16</sub>N<sub>2</sub> in the whole range spin multiplicities from 1 to 61. The computed electric polarizabilities per atom are presented in Figure 9 as a function of the spin multiplicity. As may be seen,

the polarizability curves are not monotonic with small kinks reflecting the spin flips on Fe atoms when the spin multiplicity decreases. It is quite surprising that addition of even two impurity atoms to the iron cluster results in a drastic decrease in the polarizability. Generally, the polarizability weakly depends on the spin multiplicity of a state in each series.

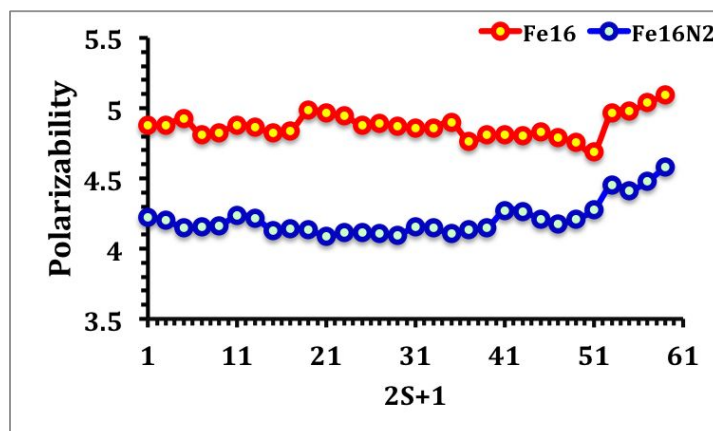


**Figure 9.** Electric polarizability per atom (in  $\text{\AA}^3$ ) of the  $\text{Fe}_{16}$  and  $\text{Fe}_{16}\text{N}_2$  clusters as a function of the spin multiplicity.

To gain insight into the dependence of computed static electric polarizability value on the method used, we performed polarizability computations using the congener BLYP method<sup>82</sup> and the B3LYP method<sup>83</sup> which contains the Hartree-Fock exchange since the accurate calculations of polarizability values can critically depend<sup>84,85,86</sup> on its inclusion. As can be seen from the results are presented in Table 1, the difference between the values computed by the three method does not exceed 7 %.

**Table 1.** Static electric polarizabilities per atom (in  $\text{\AA}^3$ ) of  $\text{Fe}_{16}$  and  $\text{Fe}_{16}\text{N}_2$  computed by using three methods and the 6-311+G\* basis set.

	BPW91	BLYP	B3LYP
$\text{Fe}_{16}$	4.87	5.02	5.24
$\text{Fe}_{16}\text{N}_2$	5.01	5.15	5.12

The polarizability of the Fe atom computed by using eight different methods and three basis sets of triple- and quadruple-zeta quality are presented in Table S1. Comparing the table entries, one can conclude that the results of computations does not critically depend on the method and basis set used.

### 3.6. Comparison of properties between Fe<sub>16</sub>, Fe<sub>16</sub>N, and Fe<sub>16</sub>N<sub>2</sub>

To trace the changes in the electronic and bonding properties due to the attachment of one and two nitrogen atoms, we computed the adiabatic electron affinities (EA) and ionization energies (IE) of neutral Fe<sub>16</sub>N and Fe<sub>16</sub>N<sub>2</sub> and compared the values obtained to the values computed<sup>59</sup> for Fe<sub>16</sub> early using the same BPW91/6-311+G\* method. The adiabatic EA and IE values were computed according to the equations:

$$EA(M) = E(M) + E_0(M) - [E(M^-) + E_0(M^-)] \quad (3)$$

$$IE(M) = E(M^+) + E_0(M^+) - [E(M) + E_0(M)] \quad (4)$$

where  $E(M)$ ,  $E(M^-)$ , and  $E(M^+)$  are total electronic energies of the lowest energy states of neutral species and its anions and cations, respectively, and  $E_0(M^q)$ ,  $q = 0, +1$ , or  $-1$ , is the zero-point vibrational energy computed in the harmonic approximation. The binding energies per atom are computed according the equation:

$$BE(M) = [16E(\text{Fe}) + kE(\text{N}) - E(M) - E_0(M)]/(16+k) \quad (5)$$

Where  $M = \text{Fe}_{16}\text{N}$ ,  $\text{Fe}_{16}\text{N}_2$  or their ions and  $k = 0, 1$ , or  $2$ . The computed and previously reported EA, IE and BE values are compared in Table 2.

**Table 2.** Ionization energies, adiabatic electronic affinities and binding energies per atom of Fe<sub>16</sub>, Fe<sub>16</sub>N, and Fe<sub>16</sub>N<sub>2</sub>.

	Fe <sub>16</sub>	Fe <sub>16</sub> N	Fe <sub>16</sub> N <sub>2</sub>
IE, eV	5.44 <sup>a</sup>	5.42	5.46
EA, eV	2.09 <sup>b</sup>	1.98	2.09
BE, eV	3.10	3.23	3.36

<sup>a</sup> Experimental values are  $5.63 \pm 0.05$  eV<sup>87</sup> and  $5.64 \pm 0.06$  eV.<sup>88</sup>

<sup>b</sup> Experimental values are  $2.01 \pm 0.08$  eV<sup>89</sup> and  $2.09 \pm 0.06$  eV.<sup>90</sup>

The single N attachment leads to a decrease in EA by 0.11 eV and returns to the value of the initial Fe<sub>16</sub> cluster after the second N is attached. The IE changes are in the limits of 0.02 eV, whereas the BE shows a substantial increase after the first and next second N atom is attached.

The binding energies of the first and second N atoms as well as of the dissociated N<sub>2</sub> dimer are computed as the difference in total energy of the initial state and the ground-state products. They are presented in Table 3.

**Table 3.** Binding energies (in eV) of N and N<sub>2</sub> in Fe<sub>16</sub>N and Fe<sub>16</sub>N<sub>2</sub> in the neutral and singly charged ground-state clusters.

Charge	Fe <sub>16</sub> N <sup>q</sup> → Fe <sub>16</sub> <sup>q</sup> +N	Fe <sub>16</sub> N <sub>2</sub> <sup>q</sup> → Fe <sub>16</sub> N <sup>q</sup> +N	Fe <sub>16</sub> N <sub>2</sub> <sup>q</sup> → Fe <sub>16</sub> <sup>q</sup> +N <sub>2</sub>
<i>q</i> = 0	5.19	5.49	0.82
<i>q</i> = -1	5.06	5.59	0.80
<i>q</i> = +1	5.18	5.54	0.79

The binding energy of the first N atom exceeds 5 eV independent of charge and is essentially larger than the binding energy of a Fe atom in Fe<sub>16</sub> or Fe<sub>17</sub> which are around 3.5 eV.<sup>59</sup> The binding energies of the second N atom increases further by 0.30 eV in the neutral case and by 0.53 eV in the cation case. The desorption energy of the N<sub>2</sub> dimer is nearly independent of the cluster charge and are relatively small (less than 20 Kcal/mol). The bond dissociation energy of the N<sub>2</sub> dimer computed at the BPW91/6-311+G\* is 9.94 eV and the sum of the binding energies of the first and second N atoms in the neutral case is 10.68 eV, therefore, the dissociation of N<sub>2</sub> on a neutral Fe<sub>16</sub> cluster is exothermic by 0.74 eV. It is also exothermic by 0.71 eV and 0.78 eV in the case of the anion and cation, respectively.

### 3.7. Simulated UV and IR spectra of Fe<sub>16</sub>N<sub>2</sub><sup>0,±1</sup>

The IR and Raman spectra of the ground-state Fe<sub>16</sub>N<sub>2</sub><sup>0,±1</sup> clusters simulated using the computed vibrational frequencies and corresponding IR intensities and Raman activities are displayed in Figure 10.

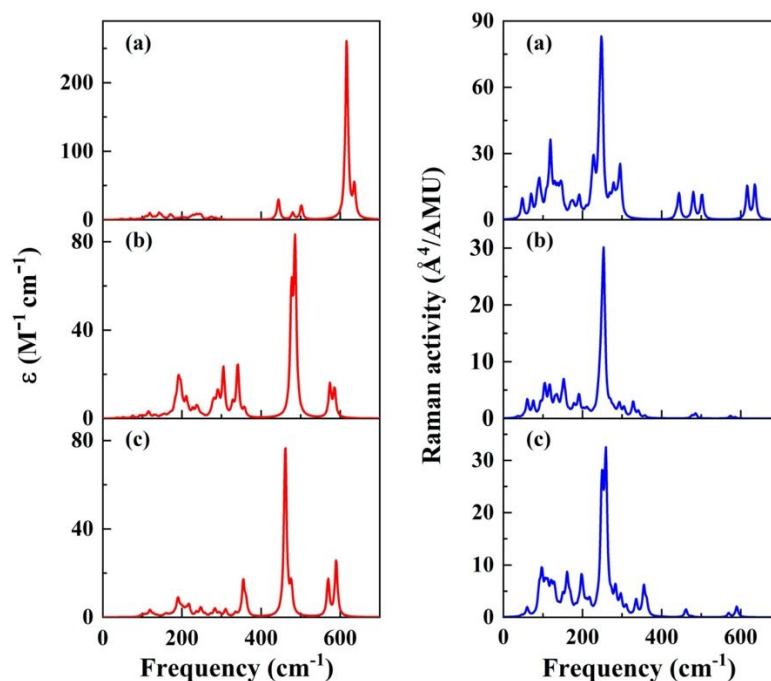


**Figure 10.** Simulated IR (the left column) and Raman (the right column) spectra of the  $\text{Fe}_{16}\text{N}_2^-$  (a),  $\text{Fe}_{16}\text{N}_2^+$  (b) and  $\text{Fe}_{16}\text{N}_2$  (c) clusters.

In the IR spectrum of each cluster, the most intense peaks are identified to be due to the symmetric vibrations of N atoms and peaks at low frequencies are mainly due to the Fe atom vibrations. In the case of the  $\text{Fe}_{16}\text{N}_2^-$  anion, the strongest peak with a shoulder located at  $616\text{ cm}^{-1}$  and  $635\text{ cm}^{-1}$  corresponds to the symmetric and asymmetric stretching modes of both N atoms. The significantly less intense features with essential contributions from the wagging N vibrations appear at frequencies of  $443\text{ cm}^{-1}$ ,  $443\text{ cm}^{-1}$ , and  $501\text{ cm}^{-1}$  whereas the vibrations at lower frequencies involve predominantly iron atoms and the corresponding peaks possess intensities by two-three orders of the magnitude smaller than the main peak intensity.

The major peak and its shoulder in the spectrum of the cationic  $\text{Fe}_{16}\text{N}_2^+$  cluster are shifted to lower frequencies of  $477\text{ cm}^{-1}$  and  $486\text{ cm}^{-1}$  and also correspond to the stretching modes of two N atoms. Note that the intensity of the major peak in the cation spectrum is about three times smaller than in the anionic case. Four peaks at  $305\text{ cm}^{-1}$ ,  $341\text{ cm}^{-1}$ ,  $574\text{ cm}^{-1}$  and  $586\text{ cm}^{-1}$  correspond to wagging vibrations of nitrogen atoms at  $242\text{ cm}^{-1}$ . In the IR spectrum of the neutral  $\text{Fe}_{16}\text{N}_2$  cluster, the strongest peak at  $461\text{ cm}^{-1}$

corresponds to the symmetrical stretching mode of both N atoms, and the shoulder at  $476\text{ cm}^{-1}$  is attributed to the asymmetrical stretching of the N atoms. The prominent peaks at  $355\text{ cm}^{-1}$ ,  $362\text{ cm}^{-1}$ ,  $569\text{ cm}^{-1}$ , and  $590\text{ cm}^{-1}$  also are due mainly to the N atom wagging vibrations. From comparing all three spectra, one may conclude that the peaks corresponding to the N atoms are fingerprints of the charged state of a  $\text{Fe}_{16}\text{N}_2$  cluster.

In the Raman spectra of all three clusters, peaks at the frequencies corresponding to the most intense peaks in the IR spectra practically disappear except for the anion case. The peak with the largest intensity in the anion spectrum is due to the overlapping peaks at  $242\text{ cm}^{-1}$ ,  $247\text{ cm}^{-1}$  and  $249\text{ cm}^{-1}$  and the most prominent peak at smaller frequencies is due to two nearly degenerate modes at  $119\text{ cm}^{-1}$ . All these peaks are due to mostly iron atom vibrations. The strongest peak of the cation is formed by the overlap of peaks at  $249\text{ cm}^{-1}$ ,  $253\text{ cm}^{-1}$  and  $254\text{ cm}^{-1}$  whereas the peaks with the strongest Raman activities in the neutral correspond to two nearly degenerate modes at  $259\text{ cm}^{-1}$  and a high intensity shoulder formed by overlapping peaks at  $249\text{ cm}^{-1}$  and  $251\text{ cm}^{-1}$  and  $260\text{ cm}^{-1}$ . As can be seen, the positions of major peaks in the spectra of the neutral and charged clusters depends weakly on charge, but the features at smaller frequencies show much larger dependence on charge.

#### 4. PECULIARITIES OF CHEMICAL BONDING IN $\text{Fe}_{16}\text{N}_2^{0,\pm 1}$

Chemical bonding of the  $\text{Fe}_{16}\text{N}_2^{0,\pm 1}$  clusters were explored by using the AdNDP method. As expected, the bonding patterns depends weakly on charge, therefore, we discuss in detail only the bonding patterns of the neutral which are shown in Figure 11 whereas the bonding patterns of the anionic  $\text{Fe}_{16}\text{N}_2^-$  and cationic  $\text{Fe}_{16}\text{N}_2^+$  clusters are presented in the Supporting Information in Figures S4 and S5, respectively.

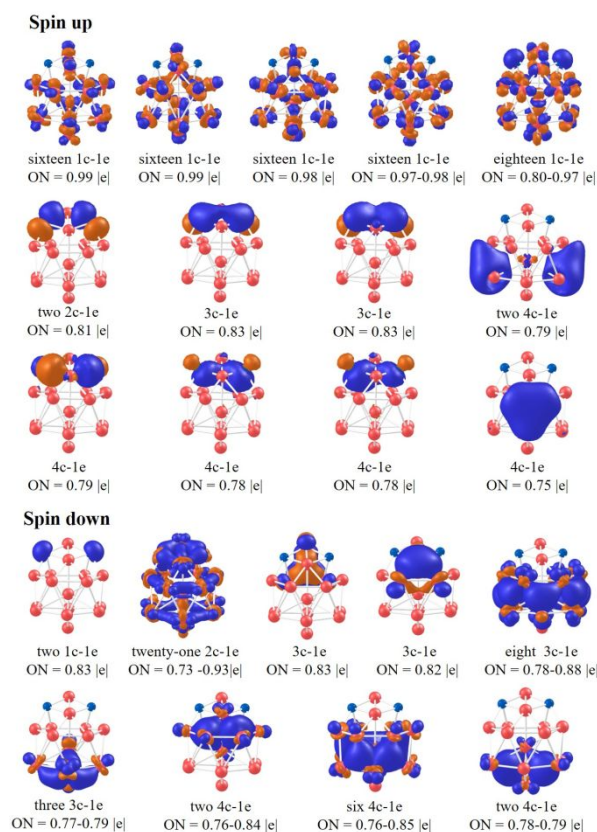


**Figure 11.** The results of our AdNDP analysis for the ground-state  $\text{Fe}_{16}\text{N}_2$  cluster in both spin-up and spin-down representations. ON denotes the occupation number.

As can be seen in Figure 11, the bonding orbitals in the spin-up ( $\alpha$ ) and spin-down ( $\beta$ ) representations are different and all local spin orbitals (LSO) but two belong to the  $\alpha$ -representation. The total number of LSOs is 84 and consists of LSOs corresponding to sixteen closed half-shells  $3d^5$  of the Fe atoms and four LSOs corresponding to  $2s^2$  subshells of the N atoms. There are ten  $\alpha$ -bonding orbitals which include two two-center ( $2c-1e$ ), two three-center ( $3c-1e$ ) and six four-center ( $4c-1e$ ) orbitals occupied by ten electrons. The spin-down representation contains a significantly richer set of bonding orbitals: twenty-one two-center, thirteen three-center, and ten four-center orbitals occupied by 44 electrons. The total number of electrons occupying all LSOs and bonding orbitals equals the sum of the number of electrons in the valence electronic configurations of iron ( $3d^64s^2$ ) and nitrogen ( $2s^22p^3$ ) atoms. Each iron LSO are occupied by one electron and may contribute one  $\mu_B$  to the total spin magnetic moment of the cluster whereas each nitrogen LSO is occupied by two electrons and there is no contribution from

these LSOs to the total spin magnetic moment. The total magnetic moment of the cluster equals the difference in the number of electrons in the  $\alpha$ - and  $\beta$ -spin representations measured in  $\mu_B$ . One may conclude that the magnetic properties of the cluster are defined primarily by the iron  $\alpha$ -LSOs and a decrease in the total spin magnetic moment from  $52 \mu_B$  in the ground-state  $\text{Fe}_{16}$  cluster to  $46 \mu_B$  in the ground-state  $\text{Fe}_{16}\text{N}_2$  cluster is due to the formation of  $\beta$ -occupied orbitals due to the associative attachment of nitrogen atoms. It is worth mentioning that exactly same patterns were found<sup>91</sup> for the  $3d$ -metal dimers but the bonding patterns in the  $\text{Fe}_{16}\text{N}_2$  are more complicated because there are multicenter bonding orbitals.

## 5. CONCLUDING REMARKS

Using density functional theory with the generalized gradient approximation and a basis set of triple- $\zeta$  quality, we performed a detailed study on the structure and properties of the  $\text{Fe}_{16}\text{N}_2$  cluster starting with coalescence of two  $\text{Fe}_8\text{N}$ . It was found that the coalescence may proceed both via transition states and corresponding energy barriers and directly without any barrier at all. The geometrical structure of resulting  $\text{Fe}_{16}\text{N}_2$  isomers was observed to depend strongly on the mutual orientation of the coalescing moieties. A similar dependence on the mutual orientation was found for the bare iron clusters  $\text{Fe}_8$  as well. The most favorable geometry of the  $\text{Fe}_{16}\text{N}_2$  cluster is that where two nitrogen atoms share a common Fe vertex which can be related to a kind of superexchange since the corresponding ferrimagnetic states where the local spin magnetic moment on the shared iron atom flips are close in total energy to the initial ferromagnetic states. Moreover, in some isomers such a ferrimagnetic arrangement of the local spin moments is the most favorable. The ground-state geometries were used in optimizations of states of both  $\text{Fe}_{16}$  and  $\text{Fe}_{16}\text{N}_2$  in the whole range spin multiplicities of  $1 \leq 2S + 1 \leq 61$ . Total energies of both clusters show a similar decrease in total energy when the spin multiplicity decreases and the  $\text{Fe}_{16}\text{N}_2$  curve approaches the  $\text{Fe}_{16}$  curve from below. In the singlet state of  $\text{Fe}_{16}$ , the atoms with parallel spin coupling form two domains reminding the domain formation in solid magnetic materials. Surprisingly, the addition

of two N atoms does not influence the local spin magnetic moment distribution. In order to estimate binding energies in the  $\text{Fe}_{16}\text{N}_2$  series consisting of the neutral and its singly charged ions, we optimized the corresponding series of  $\text{Fe}_{16}\text{N}$ ,  $\text{Fe}_{16}\text{N}^-$  and  $\text{Fe}_{16}\text{N}^+$ . It was found that the binding energies of the second N are larger than those of the first one independent of charge and they are larger than the binding energies of iron atoms in the bare  $\text{Fe}_{16}$ – $\text{Fe}_{18}$  clusters by about 2 eV. The desorption energy of a  $\text{N}_2$  dimer practically does not depend on charge and is relatively small, around 0.8 eV, which is related with the strong bond of the  $\text{N}_2$  dimer. The gain in total energy due to dissociation of  $\text{N}_2$  on the  $\text{Fe}_{16}$  cluster is mostly compensated by the energy required to break the bond in the nitrogen dimer. It is curious that the dipole electric polarizability of  $\text{Fe}_{16}$  decreases substantially when two N atoms are added. Another curious finding is that IR spectra may be used as fingerprints of a charge on a  $\text{Fe}_{16}\text{N}_2$  cluster. The chemical bonding in the  $\text{Fe}_{16}\text{N}_2$ ,  $\text{Fe}_{16}\text{N}_2^-$  and  $\text{Fe}_{16}\text{N}_2^+$  was explored using the AdNDP method which allows the construction of localized multi-center bonding orbitals. In the neutral case, there are ten bonding orbitals in the spin majority representation and 44 in the minority spin representation. Such a disparity is due to the fact that the majority spin representation contains sixteen half-filled 3d-subshells of iron atoms which are responsible for the large magnetic moment in the ferromagnetic state and are chemically inert.

#### **ACKNOWLEDGEMENT**

This work was supported by the National Natural Science Foundation of China (Nos. 11874043, 11574220, U1804121 and 11304167), and the Program for Science & Technology Innovation Talents in Universities of Henan Province (No. 15HASTIT020). Portions of this research were conducted with high-performance computational resources, provided by the Louisiana Optical Network Infrastructure (<http://www.loni.org>). G.L.G. acknowledges the support of the U.S. Army Research Office through Contract W911NF-19-1-0099. B.R.R. acknowledges the support from the National Science Foundation under Grant Number OIA-1541079. The work has been performed in accordance with the Russian Government state task (State registration No. AAAA-A19-119092390076-7).

## References

- <sup>1</sup> J. P. Wang, Environment-Friendly Bulk Fe<sub>16</sub>N<sub>2</sub> Permanent Magnet: Review and Prospective. *J. Magn. Mater.*, 2020, **497**, 165962.
- <sup>2</sup> Y. J. Shi, Y. L. Du and G. Chen, First-Principles Study on the Elastic and Electronic Properties of Hexagonal ε-Fe<sub>3</sub>N. *Comput. Mater. Sci.*, 2013, **67**, 341-345.
- <sup>3</sup> N. Ji, M. S. Osofsky, V. Lauter, L. F. Allard, X. Li, K. L. Jensen, H. Ambaye, E. Lara-Curzio and J. P. Wang, Perpendicular Magnetic Anisotropy and High Spin-Polarization Ratio in Epitaxial Fe-N thin films. *Phys. Rev. B*, 2011, **84**, 245310.
- <sup>4</sup> N. Ji, V. Lauter, X. W. Zhang, H. Ambaye and J. P. Wang, Strain Induced Giant Magnetism in Epitaxial Fe<sub>16</sub>N<sub>2</sub> Thin Film. *Appl. Phys. Lett.*, 2013, **102**, 072411.
- <sup>5</sup> Y. F. Jiang, M. A. Mehedi, E. G. Fu, Y. Q. Wang, L. F. Allard and J. P. Wang, Synthesis of Fe<sub>16</sub>N<sub>2</sub> Compound Free-Standing Foils with 20 MGOe Magnetic Energy Product by Nitrogen Ion-Implantation. *Sci. Rep.*, 2016, **6**, 25436.
- <sup>6</sup> J. M. Liu, G. N. Guo, X. W. Zhang, F. Zhang, B. Ma and J. P. Wang, Synthesis of α''-Fe<sub>16</sub>N<sub>2</sub> Foils with an Ultralow Temperature Coefficient of Coercivity for Rare-Earth-Free Magnets. *Acta Mater.*, 2020, **184**, 143-150.
- <sup>7</sup> M. N. Leuenberger and D. Loss, Quantum Computing in Molecular Magnets. *Nature*, 2001, **410**, 789-793.
- <sup>8</sup> Z. Ye, P. Zhang, X. Lei, X. Wang, N. Zhao and H. Yang, Iron Carbides and Nitrides: Ancient Materials with Novel Prospects, *Chem-Eur. J.*, 2018, **24**, 8922-8940.
- <sup>9</sup> L. Wu, R. Tian, B. Wan, H. Liu, N. Gong, P. Chen, T. Shen, Y. Yao, H. Gou and F. Gao, Prediction of Stable Iron Nitrides at Ambient and High Pressures with Progressive Formation of New Polynitrogen Species. *Chem. Mater.*, 2018, **30**, 8476–8485.
- <sup>10</sup> T. K. Kim and M. Takahashi, New Magnetic Material Having Ultrahigh Magnetic Moment. *Appl. Phys. Lett.*, 1972, **20**, 492-494.
- <sup>11</sup> Y. Sugita, K. Mitsuoka, M. Komuro, H. Hoshiya, Y. Kozono and M. Hanazono, Giant Magnetic Moment and Other Magnetic Properties of Epitaxially Grown Fe<sub>16</sub>N<sub>2</sub> Single-Crystal Films. *J. Appl. Phys.*, 1991, **70**, 5977-5982.
- <sup>12</sup> H. Tanaka, H. Harima, T. Yamamoto and Y. Katayama, Electronic Band Structure and Magnetism of Fe<sub>16</sub>N<sub>2</sub> Calculated by the FLAPW Method. *Phys. Rev. B*, 2000, **62**, 15042-15046.
- <sup>13</sup> N. Ji, X. Liu and J. P. Wang, Theory of Giant Saturation Magnetization in Fe<sub>16</sub>N<sub>2</sub>: Role of Partial Localization in Ferromagnetism of 3d Transition Metals. *New J. Phys.*, 2010, **12**, 063032.

- 
- <sup>14</sup> H. Sims, W. H. Butler, M. Richter, K. Koepf, E. Sasioglu, C. Friedrich and S. Blugel, Theoretical Investigation into the Possibility of Very Large Moments in Fe<sub>16</sub>N<sub>2</sub>. *Phys. Rev. B*, 2012, **86**, 174422.
- <sup>15</sup> M. Castro and D. R. Salahub, Density-functional Calculations for Small Iron Clusters: Fe<sub>n</sub>, Fe<sub>n</sub><sup>+</sup>, and Fe<sub>n</sub><sup>-</sup> for n ≤ 5. *Phys. Rev. B*, 1994, **49**, 11842-11852.
- <sup>16</sup> O. Diéguez, M. M. G. Alemany, C. Rey, P. Ordejón and L. J. Gallego, Density-Functional Calculations of the Structures, Binding Energies, and Magnetic Moments of Fe Clusters with 2 to 17 Atoms. *Phys. Rev. B*, 2001, **63**, 205407.
- <sup>17</sup> G. L. Gutsev, Key Role of Antiferromagnetic States in Remagnetization of Iron Clusters. *Phys. Rev. B*, 2002, **65**, 132417.
- <sup>18</sup> P. Bodabova-Parvanova, K. A. Jackson, S. Srinivas, M. Horoi, C. Kohler and G. Seifert, Scanning the Potential Energy Surface of Iron Clusters: A Novel Search Strategy. *J. Chem. Phys.*, 2002, **116**, 3576–3587.
- <sup>19</sup> G. L. Gutsev and C. W. Bauschlicher, Jr., Electron Affinities, Ionization Energies, and Fragmentation Energies of Fe<sub>n</sub> clusters (n = 2 – 6): a Density Functional Theory Study, *J. Phys. Chem. A*, 2003, **107**, 7013-7023.
- <sup>20</sup> Z. Sljivančanin and A. Pasquarello, Supported Fe Nanoclusters: Evolution of Magnetic Properties with Cluster Size. *Phys. Rev. Lett.*, 2003, **90**, 247202.
- <sup>21</sup> P. Calaminici, Polarizability of Fe<sub>n</sub> (n ≤ 4) Clusters: An All-Electron Density Functional Study. 2004, **387**, 253-257.
- <sup>22</sup> S. Yu, S. Chen, W. Zhang, L. Yu and Y. Yin, Theoretical Study of Electronic Structures and Magnetic Properties in Iron Clusters (n ≤ 8). *Chem. Phys. Lett.*, 2007, **446**, 217–222.
- <sup>23</sup> G. Rollmann, P. Entel and S. Sahoo, Competing Structural and Magnetic Effects in Small Iron Clusters. *Comput. Mater. Sci.*, 2006, **35**, 275–278.
- <sup>24</sup> D. R. Roy, R. Robles and S. N. Khanna, Magnetic Moment and Local Moment Alignment in Anionic and/or Oxidized Fe<sub>n</sub> Clusters. *J. Chem. Phys.*, 2010, **132**, 194305.
- <sup>25</sup> K. Cervantes-Salguero and J. M. Seminario, Structure and Energetics of Small Iron Clusters. *J. Mol. Model.*, 2012, **18**, 4043–4052.
- <sup>26</sup> M. Niemeyer, K. Hirsch, V. Zamudio-Bayer, A. Langenberg, M. Vogel, M. Kossick, C. Ebrecht, K. Egashira, A. Terasaki, T. Möller, B. v. Issendorff and J. T. Lau, Spin Coupling and Orbital Angular Momentum Quenching in Free Iron Clusters. *Phys. Rev. Lett.*, 2012, **108**, 057201.
- <sup>27</sup> H. K. Yuan, H. Chen, A. L. Kuang, C. L. Tian and J. Z. Wang, The Spin and Orbital Moment of Fe<sub>n</sub> (n = 2–20) Clusters. *J. Chem. Phys.*, 2013, **139**, 034314.

- <sup>28</sup> E. Kim, A. Mohrland, P. F. Weck, T. Pang, K. R. Czerwinski and D. Tománek, Magic Numbers in Small Iron Clusters: A First-Principles Study. *Chem. Phys. Lett.*, 2014, **613**, 59–63.
- <sup>29</sup> M. Stamenova, J. Simoni and S. Sanvito, Role of Spin-Orbit Interaction in the Ultrafast Demagnetization of Small Iron Clusters. *Phys. Rev. B*, 2016, **94**, 014423.
- <sup>30</sup> M. Sakurai, K. Watanabe, K. Sumiyama and K. Suzuki, Magic Numbers in Transition Metal (Fe, Ti, Zr, Nb, and Ta) Clusters Observed by Time-of-Flight Mass Spectrometry. *J. Chem. Phys.*, 1999, **111**, 235–238.
- <sup>31</sup> G. L. Gutsev, K. G. Belay, L. G. Gutsev and C. A. Weatherford, Modification of Magnetic Properties of Iron Clusters by Doping and Adsorption: From a Few Atoms to Nanoclusters. (Springer International Publishing, 2016).
- <sup>32</sup> X. Li, K. H. Bowen, Jr., P. Jena and A. K. Kandalam, Photoelectron Spectroscopic Study of Iron-Pyrene Cluster Anions. *J. Chem. Phys.*, 2011, **135**, 204301.
- <sup>33</sup> C. P. McNary and P. B. Armentrout, Iron cluster–CO Bond Energies from the Kinetic Energy Dependence of the  $\text{Fe}_n^+$  ( $n = 4\text{--}17$ ) + CO Association Reactions. *Phys. Chem. Chem. Phys.*, 2014, **16**, 26467.
- <sup>34</sup> X. Zhang, Z. Lu, D. Ma and Z. Yang, Adsorption and Dissociation of Ammonia on Small Iron Clusters. *Int. J. Hydrogen Energy*, 2015, **40**, 346–352.
- <sup>35</sup> P. Limon, A. Miralrio and M. Castro, Adsorption and Dissociation of Carbon Monoxide on Iron and Iron-Carbon Clusters:  $\text{Fe}_n + 2\text{CO}$  and  $\text{Fe}_n\text{C} + 2\text{CO}$ ,  $n = 4$  and  $7$ . A Theoretical Study. *Comp. Theor. Chem.*, 2018, **1129**, 37–47.
- <sup>36</sup> D. M. Kiaw, V. Chernyy, J. Oomens, W. J. Buma, Z. Jamshidi, L. Visscher, L. B. F. M. Waters and J. M. Bakker, Water Dissociation upon Adsorption onto Free Iron Clusters Is Size Dependent. *J. Phys. Chem. Lett.*, 2016, **7**, 2381–2387.
- <sup>37</sup> H. Zhang, C. Cui and Z. Luo, The Doping Effect of 13-Atom Iron Clusters on Water Adsorption and O–H Bond Dissociation. *J. Phys. Chem. A*, 2019, **123**, 4891–4899.
- <sup>38</sup> C. W. Copeland, M. A. Ashraf, E. M. Boyle and R. B. Metz, Vibrational Spectroscopy of  $\text{Fe}_3^+(\text{CH}_4)_n$  ( $n = 1\text{--}3$ ) and  $\text{Fe}_4^+(\text{CH}_4)_4$ . *J. Phys. Chem. A*, 2017, **121**, 2132–2137.
- <sup>39</sup> F. Pahlavan and A. H. Pakiari, DFT Study of The Chlorine Promotion Effect on the Ethylene Adsorption over Iron Clusters. *J. Mol. Graph. Model.*, 2016, **66**, 58–66.
- <sup>40</sup> M. Castro and P. Mareca, Theoretical Study of Neutral and Charged  $\text{Fe}_7\text{-(C}_6\text{H}_6)_m$ ,  $m = 1, 2$  Rice-Ball Clusters. *J. Phys. Chem. A*, 2014, **118**, 5548–5558.

- <sup>41</sup> M. L. Weichman, J. A. DeVine and D. M. Neumark, High-Resolution Photoelectron Imaging Spectroscopy of Cryogenically Cooled  $\text{Fe}_4\text{O}^-$  and  $\text{Fe}_5\text{O}^-$ . *J. Chem. Phys.*, 2016, **145**, 054302.
- <sup>42</sup> P. Limon, A. Miralrio and M. Castro, Characterization of Magnetic Series of Iron-Carbon Clusters  $\text{Fe}_n\text{C}^{0,\pm 1}$  ( $n \leq 13$ ). *J. Phys. Chem. C*, 2020, **124**, 9484–9495.
- <sup>43</sup> P. B. Armentrout, Chapter 6. Reactivity and Thermochemistry of Transition Metal Cluster Cations in *Nanoclusters: A Bridge Across Disciplines*, Elsevier, Amsterdam, 2010.
- <sup>44</sup> G. V. Chertihin, L. Andrews and M. Neurock, Reactions of Laser-Ablated Iron Atoms with Nitrogen Atoms and Molecules. Matrix Infrared Spectra and Density Functional Calculations of Novel Iron Nitride Molecules. *J. Phys. Chem.*, 1996, **100**, 14609-14617.
- <sup>45</sup> K. Aiuchi and K. Shibuya, Jet-Cooled Optical Spectroscopy of FeN between 16 300 and 21 600  $\text{cm}^{-1}$ . *J. Mol. Spectr.*, **2000**, **204**, 235–261.
- <sup>46</sup> P. M. Sheridan, L. M. Ziurys and T. Hirano, Rotational Rest Frequencies for FeN ( $X^2\Delta_i$ ) and Revised Spectroscopic Constants for FeC ( $X^3\Delta_i$ ). *Astrophys. J.*, 2003, **593**, L141–L144.
- <sup>47</sup> A. Fiedler and S. Iwata, Portrait of Diatomic FeN. A Theoretical Study. *Chem. Phys. Lett.*, 1997, **271**, 143-151.
- <sup>48</sup> G. L. Gutsev, M. D. Mochena and C. W. Bauschlicher, Jr., Dissociative and Associative Attachment of CO,  $\text{N}_2$ , and NO to Iron Clusters  $\text{Fe}_4$ ,  $\text{Fe}_4^-$ , and  $\text{Fe}_4^+$ . *Comp. Lett.*, 2006, **2**, 220-229.
- <sup>49</sup> A. H. Pakiari and M. Mousavi, A Detailed Study of the Electronic Structure of  $\text{Fe}_3$  Cluster and Associative Adsorption of  $\text{N}_2$  to This Cluster: A Natural Bond Orbital Analysis. *J. Phys. Chem. A*, 2010, **114**, 10209–10216.
- <sup>50</sup> Z. Li and Z. Zhao, Structures, Stability, Magnetic Moments and Growth Strategies of the  $\text{Fe}_n\text{N}$  ( $n = 1-7$ ) Clusters: All-Electron Density Functional Theory Calculations. *Mater. Chem. Phys.*, 2017, **187**, 0254-0584.
- <sup>51</sup> B. L. Chen, W. G. Sun, X. Y. Kuang, G. L. Gutsev and C. Lu, Modification of Geometric and Electronic Structures of Iron Clusters by Nitrogen:  $\text{Fe}_8^-$  vs  $\text{Fe}_8\text{N}^-$ . *J. Phys. Chem. C*, 2020, **124**, 3867-3872.
- <sup>52</sup> D. Yu. Zubarev and A. I. Boldyrev, Developing Paradigms of Chemical Bonding: Adaptive Natural Density Partitioning. *Phys. Chem. Chem. Phys.*, 2008, **10**, 5207-5217.
- <sup>53</sup> Gaussian 09, Revision D.01, M. J. Frisch, G. W. Trucks, H. B. Schlegel, G. E. Scuseria, M. A. Robb, J. R. Cheeseman, G. Scalmani, V. Barone, G. A. Petersson, H. Nakatsuji, X. Li, M. Caricato, A. Marenich, J. Bloino, B. G. Janesko, R. Gomperts, B. Mennucci, H. P. Hratchian, J. V. Ortiz, A. F. Izmaylov, J. L. Sonnenberg, D. Williams-Young, F. Ding, F. Lipparini, F. Egidi, J. Goings, B. Peng, A. Petrone, T. Henderson, D. Ranasinghe, V. G. Zakrzewski, J. Gao, N. Rega, G. Zheng, W. Liang, M. Hada, M. Ehara,

---

K. Toyota, R. Fukuda, J. Hasegawa, M. Ishida, T. Nakajima, Y. Honda, O. Kitao, H. Nakai, T. Vreven, K. Throssell, J. A. Montgomery, Jr., J. E. Peralta, F. Ogliaro, M. Bearpark, J. J. Heyd, E. Brothers, K. N. Kudin, V. N. Staroverov, T. Keith, R. Kobayashi, J. Normand, K. Raghavachari, A. Rendell, J. C. Burant, S. S. Iyengar, J. Tomasi, M. Cossi, J. M. Millam, M. Klene, C. Adamo, R. Cammi, J. W. Ochterski, R. L. Martin, K. Morokuma, O. Farkas, J. B. Foresman, and D. J. Fox, Gaussian, Inc., Wallingford CT, 2016.

<sup>54</sup> A. D. Becke, Density-functional exchange-energy approximation with correct asymptotic behavior. *Phys. Rev. A*, 1988, **38**, 3098-3100.

<sup>55</sup> J. P. Perdew and Y. Wang, Accurate and simple analytic representation of the electron-gas correlation energy, *Phys. Rev. B*, 1992, **45**, 13244-13249.

<sup>56</sup> L. A. Curtiss, M. P. McGrath, J.-P. Blaudeau, N. E. Davis, R. C. Binning, Jr. and L. Radom, Extension of Gaussian-2 theory to molecules containing third-row atoms Ga–Kr. *J. Chem. Phys.*, 1995, **103**, 6104-6113.

<sup>57</sup> L. G. Gutsev, S. M. Aldoshin and G. L. Gutsev, Basis-Dependent Back Donation Effects in ZnO Nanocluster Calculations. *J. Comp. Chem.* 2020, **41**, 2583–2590.

<sup>58</sup> G. L. Gutsev, C. W. Bauschlicher, Jr., H.-J. Zhai and L.-S. Wang, Structure of  $\text{Fe}_n\text{O}$  and  $\text{Fe}_n\text{O}^-$  Clusters ( $n = 2 - 6$ ) from Photoelectron Spectroscopy and Density Functional Theory Studies. *J. Chem. Phys.*, 2003, **119**, 11135-11145.

<sup>59</sup> G. L. Gutsev, C. A. Weatherford, P. Jena, E. Johnson and B. R. Ramachandran, Structure and Properties of  $\text{Fe}_n$ ,  $\text{Fe}_n^-$ , and  $\text{Fe}_n^+$  Clusters,  $n = 7-20$ . *J. Phys. Chem. A*, 2012, **116**, 10218-10228.

<sup>60</sup> S. Li and D. A. Dixon, Molecular Structures and Energetics of the  $(\text{TiO}_2)_n$  ( $n = 1-4$ ) Clusters and Their Anions. *J. Phys. Chem. A*, 2008, **112**, 6646–6666.

<sup>61</sup> H.-J. Zhai, S. Li, D. A. Dixon and L.-S. Wang, Probing the Electronic and Structural Properties of Chromium Oxide Clusters  $(\text{CrO}_3)_n^-$  and  $(\text{CrO}_3)_n$  ( $n = 1-5$ ): Photoelectron Spectroscopy and Density Functional Calculations. *J. Am. Chem. Soc.*, 2008, **130**, 5167-5167.

<sup>62</sup> S. Li, J. M. Hennigan, D. A. Dixon and K. A. Peterson, Accurate Thermochemistry for Transition Metal Oxide Clusters. *J. Phys. Chem. A*, 2009, **113**, 7861-7877.

<sup>63</sup> F. Grein, Ground and Low-Lying Excited  $\text{C}_{2v}$  States of  $\text{FeO}_2$  – A Challenge to Computational Methods. *Int. J. Quantum Chem.*, 2009, **109**, 549-558.

<sup>64</sup> M. Ju, J. Lv, X.-Y. Kuang, L.-P. Ding, C. Lu, J.-J. Wang, Y.-Y. Jin and G. Maroulis, Systematic Theoretical Investigation of Geometries, Stabilities and Magnetic Properties of Iron Oxide Clusters  $(\text{FeO})_n^\mu$  ( $n = 1-8$ ,  $\mu = 0, \pm 1$ ): Insights and Perspectives. *RSC Adv.*, 2015, **5**, 6560- 6570.

- <sup>65</sup> G. L. Gutsev, K. G. Belay, L. G. Gutsev, B. R. Ramachandran, Geometrical and Magnetic Structure of Iron Oxide Clusters (FeO)<sub>n</sub> for n > 10. *Comp. Mater. Sci.*, 2017, **137**, 134-143.
- <sup>66</sup> J. P. Perdew, J. A. Chevary, S. H. Vosko, K. A. Jackson, M. R. Pederson, D. J. Singh and C. Fiolhais, Atoms, Molecules, Solids, and Surfaces: Applications of the Generalized Gradient Approximation for Exchange and Correlation. *Phys. Rev. B*, 1992, **46**, 6671-6687.
- <sup>67</sup> J. P. Perdew, K. Burke and M. Ernzerhof, M. Generalized Gradient Approximation Made Simple. *Phys. Rev. Lett.*, 1996, **77**, 3865-3868.
- <sup>68</sup> J. P. Perdew, A. Ruzsinszky, G. I. Csonka, L. A. Constantin and J. Sun, J. Workhorse Semilocal Density Functional for Condensed Matter Physics and Quantum Chemistry. *Phys. Rev. Lett.*, 2009, **103**, 026403.
- <sup>69</sup> Y. Zhao and D. G. Truhlar, A New Local Density Functional for Main-Group Thermochemistry, Transition Metal Bonding, Thermochemical Kinetics, and Noncovalent Interactions. *J. Chem. Phys.*, 2006, **125**, 194101.
- <sup>70</sup> J. Lv, Y. Wang, L. Zhu and Y. Ma, An Effective Structure Prediction Method for Layered Materials Based on 2D Particle Swarm Optimization Algorithm. *J. Chem. Phys.*, 2012, **137**, 084104.
- <sup>71</sup> S. Berski, G. L. Gutsev, M. D. Mochena and J. Andrés, Toward Understanding the Electron Density Distribution in Magnetic Clusters: Insight from the ELF and AIM Analyses of Ground-State Fe<sub>4</sub>, *J. Phys. Chem. A*, 2004, **108**, 6025-6031.
- <sup>72</sup> E. D. Glendening, A. E. Reed, J. E. Carpenter and F. Weinhold, NBO Version 3.1.
- <sup>73</sup> B. V. Reddy and S. N. Khanna, Chemically Induced Oscillatory Exchange Coupling in Chromium Oxide Clusters. *Phys. Rev. Lett.*, 1999, **83**, 3170–3173.
- <sup>74</sup> G. L. Gutsev, K. V. Bozhenko, L. G. Gutsev, A. N. Utenyshev and S. M. Aldoshin, Dependence of Properties and Exchange Coupling Constants on the Charge in the Mn<sub>2</sub>O<sub>n</sub> and Fe<sub>2</sub>O<sub>n</sub> Series, *J. Phys. Chem. A*, 2018, **122**, 5644–5655.
- <sup>75</sup> N. M. Reilly, J. U. Reveles, G. E. Johnson, S. N. Khanna and A. W. Castleman, Jr., Experimental and Theoretical Study of the Structure and Reactivity of Fe<sub>1-2</sub>O<sub>≤6</sub><sup>-</sup> Clusters with CO. *J. Phys. Chem. A*, 2007, **111**, 4158-4166.
- <sup>76</sup> E. L. Uzunova and H. Mikosch, Electronic Structure and Reactivity of Cobalt Oxide Dimers and Their Hexacarbonyl Complexes: A Density Functional Study. *J. Phys. Chem. A*, 2012, **116**, 3295- 3303.
- <sup>77</sup> G. L. Gutsev, C. A. Weatherford, P. Jena, E. Johnson and B. R. Ramachandran, Competition Between Surface Chemisorption and Cage Formation in Fe<sub>12</sub>O<sub>12</sub> Clusters. *Chem. Phys. Lett.*, 2013, **556**, 211–216.
- <sup>78</sup> T. M. Briere, M. H. F. Sluiter, V. Kumar and Y. Kawazoe, Atomic Structures and Magnetic Behavior of Mn Clusters. *Phys. Rev. B*, 2002, **66**, 064412.

- <sup>79</sup> P. Bodabova-Parvanova, K. A. Jackson, S. Srinivas and M. Horoi, Emergence of Antiferromagnetic Ordering in Mn Clusters, *Phys. Rev. A*, 2003, **67**, 061202(R).
- <sup>80</sup> G. L. Gutsev, C. A. Weatherford, B. R. Ramachandran, L. G. Gutsev, W. J. Zheng, O. C. Thomas and K. H. Bowen, Photoelectron Spectra and Structure of the  $Mn_n^-$  Anions ( $n = 2-16$ ), *J. Chem. Phys.*, 2015, **143**, 044306.
- <sup>81</sup> A. D. Buckingham, Finding the Way Through Intermolecular Forces. Perspective on Permanent and Induced Molecular Moments and Long-Range Intermolecular Forces, *Adv. Chem. Phys.*, 1967, **12**, 107-142.
- <sup>82</sup> C. Lee, W. Yang and R. G. Parr, Development of the Colle-Salvetti Correlation-Energy Formula into A Functional of the Electron Density. *Phys. Rev. B*, 1988, **37**, 785-789.
- <sup>83</sup> P. J. Stephens, F. J. Devlin, C. F. Chabalowski and M. J. Frisch, Ab initio calculation of vibrational absorption and circular dichroism spectra using density functional force fields, *J. Phys. Chem.*, 1994, **98**, 11623-11627.
- <sup>84</sup> M. B. Oviedo, N. V. Ilawe and B. M. Wong, Polarizabilities of  $\pi$ -Conjugated Chains Revisited: Improved Results from Broken-Symmetry Range-Separated DFT and New CCSD(T) Benchmarks. *J. Chem. Theory Comput.*, 2016, **12**, 3593-3602.
- <sup>85</sup> L. Xu, A. Kumar and B. M. Wong, Linear polarizabilities and second hyperpolarizabilities of streptocyanines: results from broken-symmetry DFT and New CCSD(T) benchmarks. *J. Comp. Chem.* 2018, **39**, 2350-2359.
- <sup>86</sup> R. Zaleśny, M. Medved', S. P. Sitkiewicz, E. Matito and J. M. Luis, Can Density Functional Theory Be Trusted for High-Order Electric Properties? The Case of Hydrogen-Bonded Complexes. *J. Chem. Theory Comput.*, 2019, **15**, 3570-3579.
- <sup>87</sup> S. Yang and M. B. Knickelbein, Photoionization Studies of Transition Metal Clusters: Ionization Potentials for  $Fe_n$  and  $Co_n$ . *J. Chem. Phys.*, 1990, **93**, 1533-1539.
- <sup>88</sup> E. K. Parks, T. D. Klots and S. J. Riley, Chemical Probes of Metal Cluster Ionization Potentials. *J. Chem. Phys.*, 1990, **92**, 3813- 3826.
- <sup>89</sup> L. S. Wang, H. S. Cheng and J. Fan, J. Photoelectron spectroscopy of size-selected transition metal clusters:  $Fe_n^-$ ,  $n = 3-24$ . *J. Chem. Phys.*, 1995, **102**, 9480- 9493.
- <sup>90</sup> L. S. Wang, X. Li and H. F. Zhang, Probing the Electronic Structure of Iron Clusters Using Photoelectron Spectroscopy, *Chem. Phys.*, 2000, **262**, 53-63.
- <sup>91</sup> G. L. Gutsev and C. W. Bauschlicher, Jr., Chemical Bonding, Electron Affinity, and Ionization Energies of the Homonuclear 3d-Metal Dimers, *J. Phys. Chem. A*, 2003, **107**, 4755-4767.

